Journal of Fusion Energy (2023)42:36
https://doi.org/10.1007/s10894-023-00374-8

RESEARCH

Investigation of Tin Removal for Liquid Metal Tokamak Divertor by Low Pressure Argon Arc with Hot Tungsten Cathode System

Himanshu Mishra[1] · Tomáš Mašek[1,2] · Zdeněk Turek[1] · Martin Čada[3] · Zdeněk Hubička[3] · Pavel Kudrna[1] · Milan Tichý[1]

Accepted: 2 August 2023

Abstract
The influence of a low-pressure argon arc with a hot tungsten cathode on the thin tin film with a negative bias voltage applied during the plasma treatment was investigated to study the tin film removal from the sample surface. Samples were prepared on a stainless-steel substrate using DC magnetron sputtering and hybrid HiPIMS assisted with electron cyclotron wave resonance (ECWR). During treatment an optical emission spectroscopy was employed to detect and characterize the emission line of tin spectrum and the electron density and temperature were measured by Langmuir probe. Morphological study by a scanning electron microscope helped to gain insight to the mechanism of tin removal from the substrate. In addition, elemental compositions of tin layer before and after treatment was measured by an energy dispersive X-ray spectroscopy. We believe that this study contributes to finding a proper treatment for tin removal from plasma facing surfaces of tokamaks using tin in the liquid metal divertor.

Keywords Tin · Argon arc · Hot cathode · Optical emission spectroscopy · Langmuir probe · Scanning electron microscope

Introduction

Thermonuclear fusion is a promising source of low-emission carbon dioxide, safe, sustainable and low-waste nuclear energy. The International Thermonuclear Experimental Reactor (ITER) tokamak is the focus of research conducted in the field of international magnetic confinement fusion. The high heat flux shield protecting the vacuum vessel against plasma as the first wall is the most critical component of the blanket and must be designed to remove the surface heat flux from the plasma, reduce the nuclear effects in the vacuum vessel and protect the superconducting coils from excessive nuclear heating and radiation damage [1]. High radiation losses due to the presence of impurities are a significant issue in tokamak and its divertor. The additional heating through neutral beam injection (NBI) or the ion cyclotron resonant heating (ICRH) [2] further increases the impurity concentration. The proper choice of materials for the tokamak's first wall is therefore of utmost importance.

Construction and upcoming operation of ITER and later demonstrative power plant (DEMO) are among the greatest milestones of the European Fusion Roadmap. Most tokamaks use graphite for the heat shield [3]. It survives huge heat fluxes, however, it forms hydrocarbons, thus binding unacceptably large amounts of radioactive tritium which is the fuel in thermonuclear reactors. Metals don't suffer this, however, even the best metal (tungsten) sputters and so contaminates the plasma and does not survive thermal cycling. The use of tungsten as the plasma facing material (PFM) for the divertor region is planned for ITER [4]. Moreover, particle fluence onto the divertor in a DEMO reactor will exceed those in ITER considerably, as reported in [5]. Among various issues like implantation and other plasma material interactions, an important issue remains the physical sputtering of tungsten, especially when

✉ Himanshu Mishra
hmishra022@gmail.com

[1] Faculty of Mathematics and Physics, Charles University, 180 00 Prague, Czech Republic

[2] Faculty of Nuclear Science and Physical Engineering, Czech Technical University in Prague, 166 36 Prague, Czech Republic

[3] Institute of Physics of the Czech Academy of Sciences, 182 00 Prague, Czech Republic

Published online: 18 August 2023

extrinsic impurities are seeded to reduce the power loads on the PFM which causes cooling of the plasma and thus deterioration of the fusion performance.

A promising alternative to the conventional solid metal targets is a liquid metal divertor (LMD) [6, 7] target, in which the liquid metal, usually Li, Sn or its alloy, is fixed within a mesh-like structure by capillary forces [8]. Liquid metals aim to handle especially the transient heat pulses (ELMs, disruptions) and may also be combined with other heat flux dissipation techniques. The LMD consists of a metal liquid wetted into a substrate with a capillary porous structure (CPS) made of 0.1 mm thin molybdenum wires [9, 10]. One of the problems of the LMD technology is the redeposition of the released metal on the tokamak vessel walls. Simulations of the experiments performed in the COMPASS upgrade tokamak [11, 12] indicated that the amount of released metal can range from mg up to several grams per second depending mainly on the geometry and lithium or tin [13–16] choice. Thus, the study of the removal of the redeposited metals is therefore of prime importance.

The main objective of the article is to study the interaction of a flowing dense low temperature plasma with a surface of thin film of tin. Understanding of the mechanism of the interaction contributes to finding the best conditions which enable the removal of tin from the sample surface. The reason for selecting tin for use in tokamak liquid metal divertor is its high possibility of recycling and low tritium-retention [17].

An enhancement of the erosion yield [18, 19] of materials under plasma bombardment as a function of temperature has been reported by many researchers [20–24]. To our knowledge there exists no paper that would study the interaction of a dense low-temperature flowing plasma on a thin tin film. We hope that by means of this study we shall contribute to greater understanding of the region of plasmas close to tin surface, i.e., of the physical as well as chemical interactions between plasma and tin surface.

In this article we used hot cathode low-pressure arc plasma source. The thin tin film was deposited on stainless-steel substrate using two different methods: magnetron sputtering [25] and hybrid HiPIMS [26] sputtering assisted with electron cyclotron wave resonance plasma (ECWR). To define the experimental conditions of the tin erosion experiment we deployed optical emission spectroscopy [27] and Langmuir probe [28] as diagnostic tools. We performed consistency analysis by comparing the tin spectral lines as well as evaluation of electron temperature and electron density at different phase of experiment. The morphological study of eroded tin after flowing plasma interaction have been performed by scanning electron microscope (SEM) with energy dispersive X-ray spectroscopy (EDS).

Experimental Details

Preparation of the Samples

Tin thin films were deposited on stainless steel (ASTM AISI 304) sheet that was cut into 10 × 25 mm rectangular substrates. Before deposition, the steel substrates were submerged in acetone and ultrasonically cleaned for 15 min, afterwards they were dried and then submerged into ethyl alcohol for another 5 min. These substrates were then dried using cleanroom wipes and mounted onto a substrate holder that was able to rotate to ensure the homogeneity of deposition, as shown in Fig. 1. This holder was placed into vacuum chamber. The samples were then treated for 10 min using RF (13.56 MHz) power supply connected on the substrate holder. The ignited discharge was operated in argon (Q_{Ar} = 100 sccm) and forming gas containing 90 at. % of nitrogen + 10 at. % of hydrogen (Q_{H2+N2} = 100 sccm) at 16 Pa pressure. The power delivered into the RF discharge was 100 W and measured DC voltage self-bias on the holder was − 330 V.

We employed two deposition techniques to prepare thin film samples. The first one utilized DC magnetron sputtering and the other one hybrid HiPIMS assisted with the electron cyclotron wave resonance (ECWR) discharge. As for the target, we used a tin target from Plasmaterials Inc. with 99.99% purity with diameter of 50 mm and thickness of 6 mm. The magnetron was placed horizontally at 80 mm distance from the substrate holder facing the center of target. Consequently, we could distinguish three types of samples shown in Fig. 1. Samples had gradually increasing thickness of sputtered tin starting from samples marked with number 1, 2, etc. due to geometry of our deposition system. For all our experiments we decided to use samples from position 2.

For the DC magnetron sputtering the chamber was pumped down to a base pressure of around 10^{-4} Pa. The operating pressure was set to 1 Pa with the mass flow rate

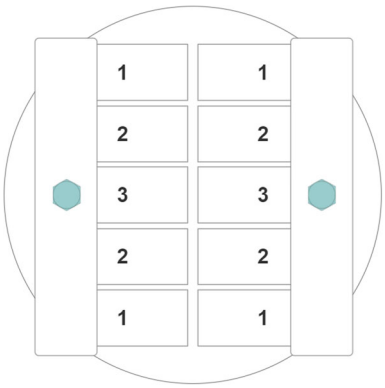

Fig. 1 Position of samples on rotating holder

of argon set to 26 sccm. The DC power was set to 50 W with deposition time of 30 min (the cathode voltage was − 376 V and the discharge current 0.13 A). For brevity we call these samples as DC samples further in the text.

For the hybrid HiPIMS sputtering the base pressure was around 10^{-3} Pa with operating pressure of 0.36 Pa and mass flow rate of argon was set to 26 sccm. The HiPIMS mode was operated with average current, I_{avg} = 70 mA. The cathode voltage pulse repetition frequency was 5 kHz, pulse on-time 20 µs, energy in one pulse 90 mJ and average power 45 W. For brevity we call these samples as HiPIMS samples further in the text.

Plasma Exposure on Thin Tin Film in Hot Cathode Configuration

The schematics of our hot cathode system and a photo of the system in operation viewed through the observation window is shown in Fig. 2. The hot cathode consists of tungsten wire of diameter 0.25 mm. We see also in Fig. 2 the cylindrical tungsten Langmuir probe (diameter 0.15 mm, length 5 mm) used for the plasma diagnostics.

Figure 3 shows the deposited tin films on the steel substrate and surface changes in the tin layer due to plasma ion bombardment. Images clearly show tin removal due to hot cathode flowing argon plasma interaction, whose detailed discussion will be done in the latter part of the paper.

Table 1 shows the research matrix used to study an effect of dense low-temperature flowing plasma on a thin tin film in argon (180 sccm) plasma. The tin samples were prepared as mentioned in Sect. "Preparation of the samples". Table 1 shows the experimental conditions, which we used for tin removal in argon plasma in a hot cathode configuration.

The cathode temperature was measured as follows; we heated the cathode by 19.45 V through which the current was measured on temperature stable 0.1 Ω resistor. This gives the value of 6.12 A. This voltage was then transferred to the cathode via wires, which unfortunately have voltage drop of 0.5–0.7 V. With the knowledge of existing voltage drop, we measure voltage on the cathode for calculating the actual resistances. The resistance of the cathode at room temperature was 0.191 Ω. From the ratio of actual resistance to that of room temperature resistance, we can calculate the temperature of the tungsten cathode using table of resistivity for tungsten as a function of temperature. Thus after heating the cathode, we apply voltage and current as shown in Table 1. By connecting the positive end of power source on the chamber and negative end on the filament we created plasma. Just under the sample substrate a thermocouple is inserted to enable in situ monitoring of the sample temperature.

Plasma diagnostics and material characterizations

We performed optical emission spectroscopy [27] and Langmuir probe [28] plasma diagnostic whose complete experimental details can be found in our previous publications. The as-prepared tin deposited thin films samples as well as the plasma-treated samples were characterized by scanning electron microscopy (TESCAN, MIRA 3 LMH)

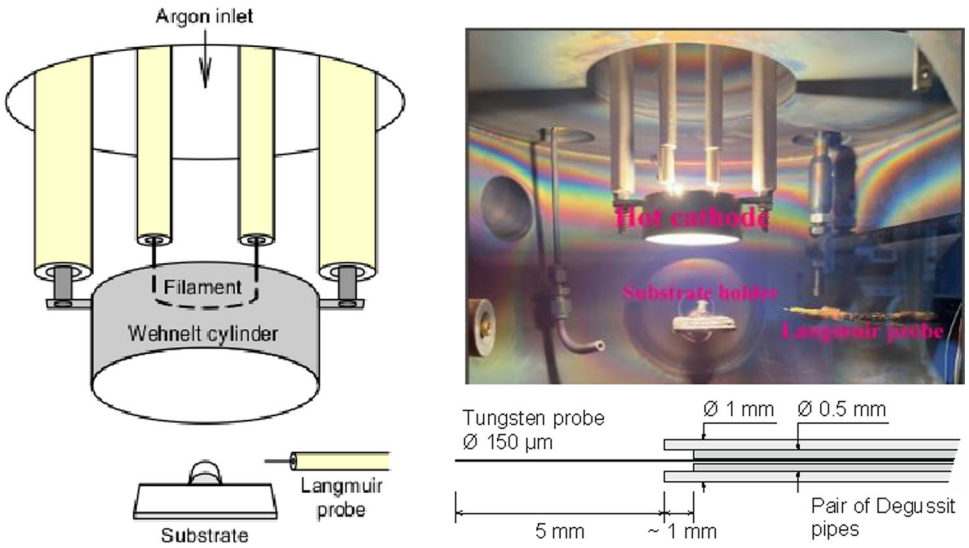

Fig. 2 Left panel: Schematics of our hot cathode system. Top right panel: Photo of hot cathode system operating in argon plasma. Pressure 1.5 Pa, discharge current 1 A, argon mass flow rate 180 sccm. Bottom right panel: Sketch of the used Langmuir probe. The OES is performed along the line of sight of substrate holder.Argon is flown from the top (tube not shown)

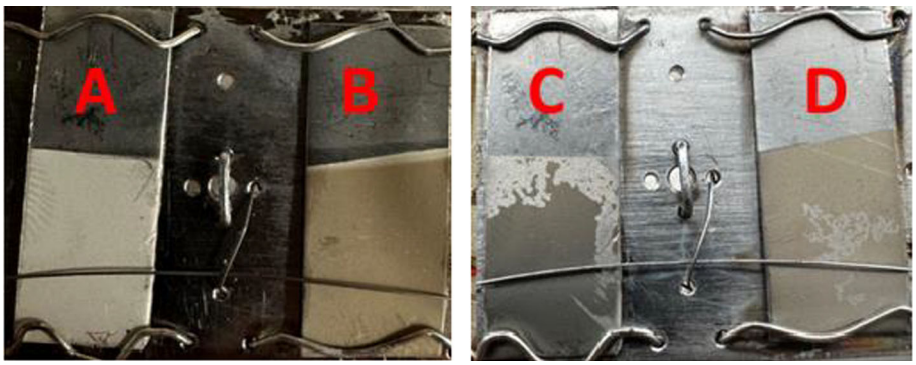

Fig. 3 Surface changes due to interaction with plasma. Left panel tin layers before interaction with argon plasma **A** DC prepared samples **B** HiPIMS prepared samples. Right panel, the same samples after interaction with argon plasma **C** DC prepared samples **D** HiPIMS prepared samples

Table 1 Research matrix for argon flowing plasma on a tin thin film deposited over steel for tin removal

Time (min)	Pressure (Pa)	Current (A)	Voltage (V)	Cathode temperature (K)	Substrate bias (V)	Current through substrate (mA)	Substrate temperature (K)
0	1.61	1	52.3	2774	− 60	47	299.06
5	1.66	1	55.7	2777	− 60	54.21	426.45
15	1.59	1	50.7	2782	− 60	49.06	469.45
25	1.64	1	45.6	2785	− 60	42.5	498.65
35	1.45	1	45.6	2785	− 60	39.61	505.15
45	1.45	1	45.8	2792	− 60	40.22	508.35
55	1.50	1	47.6	2793	− 60	41.55	511.25
65	1.48	1	47.6	2798	− 60	41.83	513.55
75	1.47	1	47.6	2796	− 60	40.2	514.05

for the morphology and energy dispersive X-ray spectroscopy (EDS) for elemental composition study.

Results and Discussions

Sputtering and Evaporation Towards PFM in Flowing Plasma

Plasma wall interactions lead to significant erosion processes at plasma facing areas. The most of erosion mechanisms are caused directly by excess heat loads, like evaporation or sublimation. However, the important erosion mechanisms are linked to the particle fluxes to the wall: physical sputtering [29, 30] and chemical reactions.

Erosion processes release particles from the wall, which can be excited, dissociated or ionized when entering the plasma [31]. Thus the resultant erosion flux (particles s^{-1}) is then either part of the plasma or lost on the chamber walls.

However, those values measured from the erosion flux cannot be explained from physical sputtering and evaporation alone. Due to high redeposition [17, 32], fraction of signal increase may be due to self-sputtering by tin, which

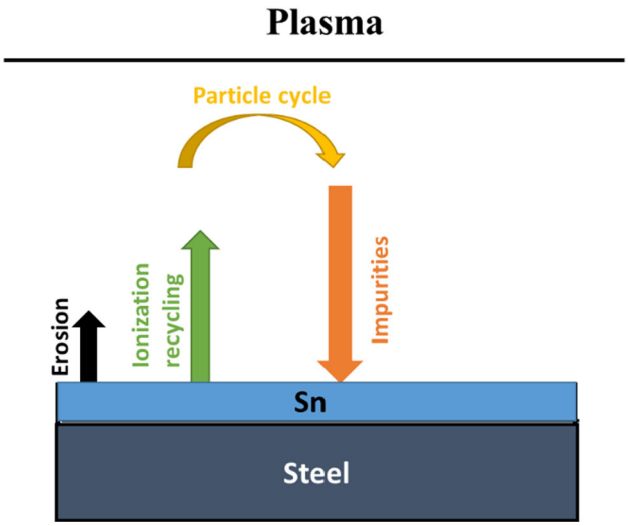

Fig. 4 Mechanism of sputtered particle trajectory in plasma

can thus liberate more tin in an ongoing cycle as shown in Fig. 4.

Optical Emission Spectroscopy Study for Eroded Tin in Argon Plasma

When tin coated substrate is exposed to argon plasma in hot-cathode environment, its surface would be eroded mainly by evaporation and sputtering process. Most evaporated and sputtered tin atoms from the thin layer could form a vapor cloud above the layer surface with a high re-deposition rate [21]. The atoms of tin could be ionized through collision with the electron and other incident particles forming tin ions in an unstable excited state that relax to ground state while radiating photons with different energy. However, some tin atoms are not ionized by the plasma and condense at the chamber wall and substrate holder; and the process of sputtering, evaporations and self-sputtering is repeated.

The whole set of experiment data was collected in time span of 75 min with gap of 10 min each. The main data relevant to tin sputtering are the particle identity, the concentration, and the energy of the sputtering particles. Further the fraction of the sputtered particles that really leave the surface, i.e., are not promptly redeposited. The spectrum intensity of tin could reveal the quantity of ionized tin ions. Tin spectral lines Sn I 365.5 nm, Sn I 380.1 nm, Sn I 452.5 nm, Sn II 805.5 nm, Sn I 811.4 nm were captured through OES spectra as shown in Fig. 5. These spectral lines were taken from NIST Atomic Spectra Database Lines Data [33]. In Fig. 5 it can be seen that the intensity of spectral lines increases with the increase of surface temperature. For clarity in OES spectra, in Fig. 5 we show here low and high temperature values. This depicts that plasma approaches dynamic equilibrium as temperature increases. The dynamic equilibrium means there are some tin atoms which are not ionized and get condensed at low temperature part of chamber while in parallel there are ionization of tin atoms took places abruptly. The one of prominent reason for the increase in tin removal is an abnormal enhanced erosion phenomenon depending on the surface temperature [17, 21]. More detail discussion on tin erosion will be done later in Sect. "Surface Morphological Study for Thin Tin Film".

Figure 6 shows the logarithm of spectrum intensity value vs inverse of temperature for various tin spectral lines. It depicts that the spectral intensity increases with increase in temperature. The increase in intensity can be attributed to the removal of tin from the layer on the stainless-steel substrate in plasma. To describe the significantly enhanced erosion by sublimation/evaporation and sputtering at high temperature, a model based on superficial adsorbed atoms was proposed and the total erosion rate could be written as below [21]:

$$R(T) = \mathrm{k}_{no}\mathrm{n}_o exp\left(-\frac{E_0}{K_B T}\right) + \Gamma_{ion} Y_{ps} + \Gamma_{ion} Y_{eff} exp\left(-\frac{E_{eff}}{K_B T}\right)$$

Here $\mathrm{k}_{no}\mathrm{n}_o exp\left(-\frac{E_0}{K_B T}\right)$ represents classical evaporation, k_{no} is constant, n_o is the surface density of lattice atoms, K_B is the Boltzmann constant, T is the tin surface temperature, E_0 is the binding energy of materials. $\Gamma_{ion} Y_{ps}$ is physical sputtering rate (Y_{ps} is the physical sputtering yield and Γ_{ion} is the incident particle flux). $\Gamma_{ion} Y_{eff} exp\left(-\frac{E_{eff}}{K_B T}\right)$ represents the enhanced erosion rate induced by adsorption atomic evaporation, and E_{eff} is the measured surface binding energy (sublimation energy), which could be obtained by Arrhenius plot fitting of the enhanced region. Figure 7 shows the logarithm of spectral intensity vs inverse of

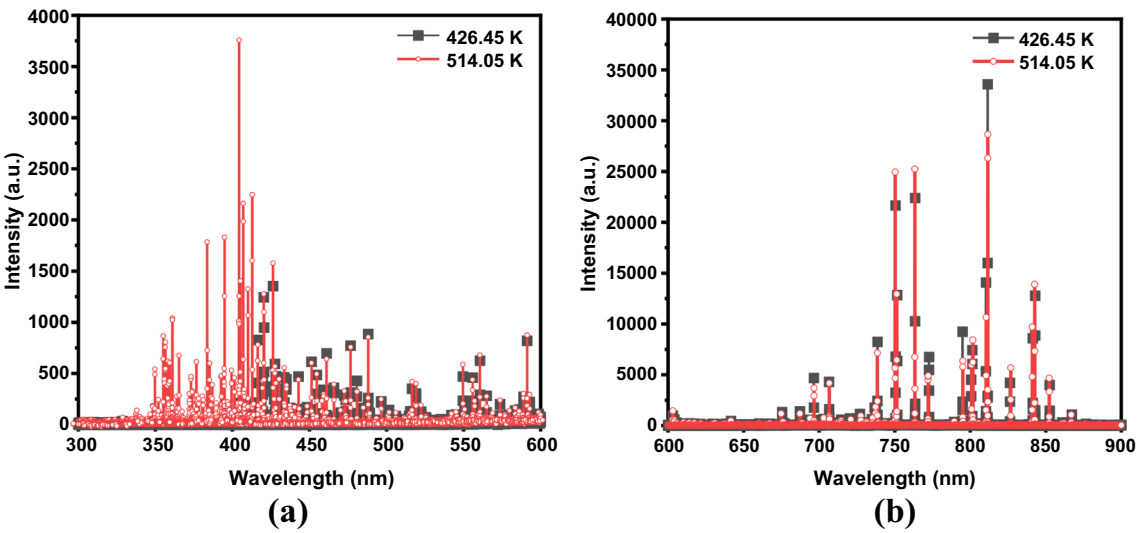

Fig. 5 Optical emission spectra for eroded tin in argon plasma for low and high temperature **a** for 300–600 nm **b** for 600–900 nm

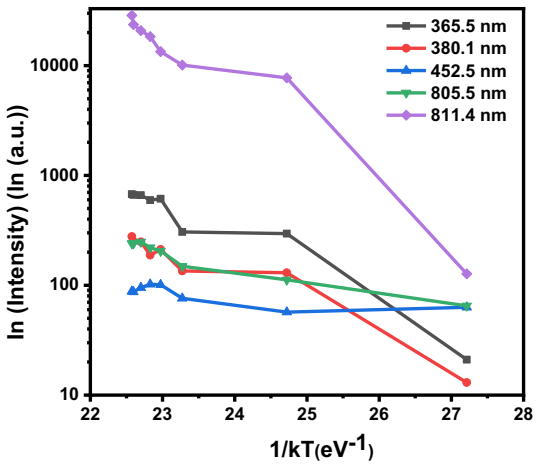

Fig. 6 The logarithm of spectrum intensity plotted against inverse of kT

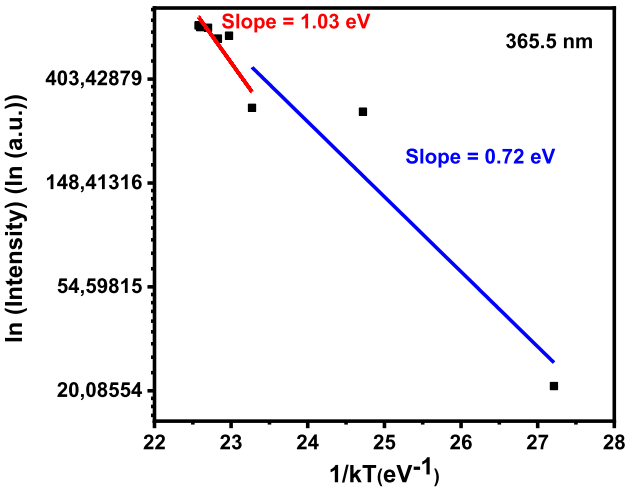

Fig. 7 The logarithm of spectrum intensity plotted against inverse of kT for the 365.5 nm line. The error range is 1.03 ± 0.25 eV and 0.72 ± 0.27 eV

temperature for spectral line 365.5 nm. The E_{eff} value could be extracted as the slope of the curve [21] in Fig. 7.

As shown in Fig. 7, there are two slopes obviously corresponding to high temperature stage and low temperature stage in the plasma irradiation process. When the temperature stays below the evaporation threshold, E_{eff} value is 0.72 eV, otherwise the E_{eff} value is 1.03 eV. The values of E_{eff} indicates that we are in low temperature regime. Consequently, the sputtering is main cause of tin erosion as mentioned in report [21] for given temperature range.

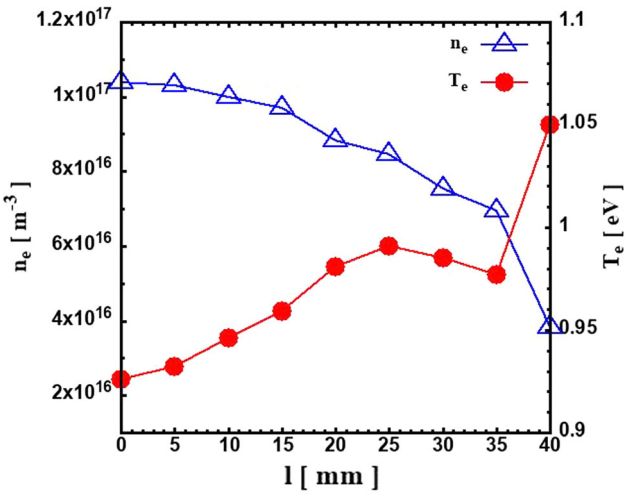

Fig. 8 Variations of the electron density and electron temperature with the distance from the chamber axis for pressure 1.5 Pa and Ar flow rate 180 sccm. Sample holder not present. Zero distance corresponds to the vacuum chamber axis. The error bar is ± 15 percent

Langmuir Probe Study for Eroded Tin in Argon Plasma

Figure 8 shows plot of the electron temperature and electron density determined by Langmuir probe. The sample holder was not inserted; hence we could measure up to the vacuum chamber axis.

The electron density decreases with increasing distance from the chamber axis as one would expect. The electron temperature reaches a rather low value at the chamber axis, 0.93 eV, due to the proximity of the hot cathode. Towards the chamber wall the electron temperature rises since the amount of thermo-emitted electrons from the cathode decreases and the hotter electrons contribute to keeping the adjusted discharge current.

The variations of the electron density and temperature with the distance from the chamber axis when substrate was inserted into the chamber are depicted in Fig. 9. When the substrate holder was inserted, we could not reach the axis with the probe. Therefore, the measurements start at the distance 15 mm from the axis. Figure 9a, b show plot of electron density and electron temperature respectively. The parameter in both plots is the time of treatment and indirectly the sample temperature. It is evident that with increasing time (sample temperature) the electron density rises while keeping the decreasing trend towards the chamber wall. The rise of electron density is accompanied by the decrease of electron temperature, which is almost constant with the distance from the axis. We attribute both the electron density increase and the electron temperature decrease to the presence of tin in the argon working gas, the concentration of tin increases with time because of rise

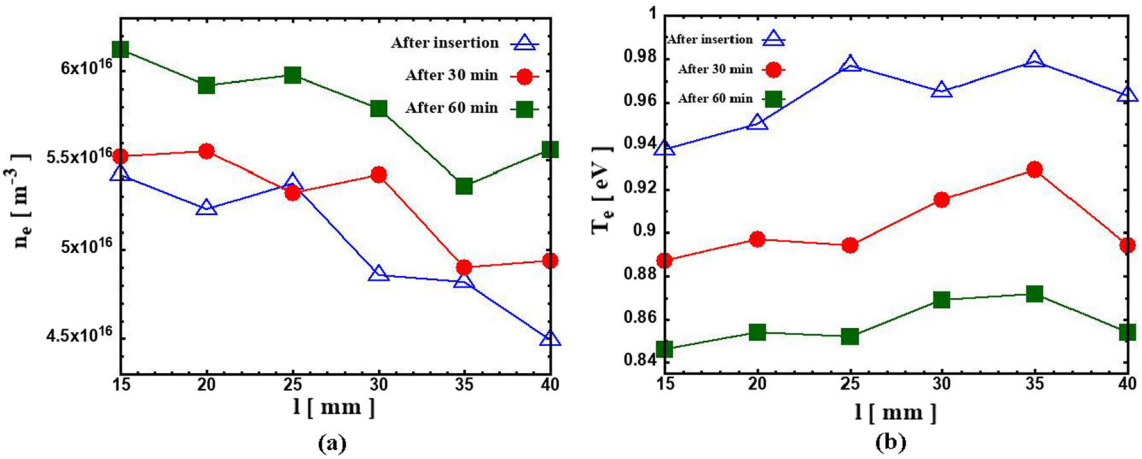

Fig. 9 Variations of electron density (**a**) and electron temperature (**b**) with the distance from the chamber axis in the presence of the sample holder with a DC sample for pressure 1.5 Pa and Ar flow rate 180 sccm. The error bar is ± 15 percent

in the sample temperature during the treatment. Also, tin has much lower ionization energy, 7.34 eV compared to argon with 15.76 eV.

Surface Morphological Study for Thin Tin Film

As we could see in Fig. 3 the interaction with plasma changes the tin surface of both samples significantly. On both samples we can distinguish two types of interaction, the first one can be found on majority of the film surface, whereas the second one affected only a small portion of it which is depicted as minority.

The detailed structure of the tin layer surface before plasma interaction is shown in Fig. 10, left panel. This layer of tin is approximately 1 μm thick. We see crystals of tin of approximately several micrometers in size. After plasma interaction most of the surface is changed as is shown in the middle panel of Fig. 10. These changes are presumably due to the sample temperature higher than tin melting point. Higher temperature melted most of the crystals and created rather homogenous surface. The ripple effect (wavy structure) which can be seen on the surface is due to interaction of the tin surface with ions [34]. The minority surface area after plasma interaction is depicted in right panel in Fig. 10. An area like that is usually found in the vicinity of border between steel and tin. As we observed also in other experiments, such an area is created in the first few minutes of interaction with plasma after applying negative bias on the samples. Therefore, we can say that this interaction is not created due to temperature but purely by interaction with ions.

The main difference between these two types of interaction can be found in energy dispersive X-ray spectroscopy (EDS) spectrum in Fig. 11. On majority of the sample surface, we observe only small change of thickness of tin layer, which is due to destruction of crystalline

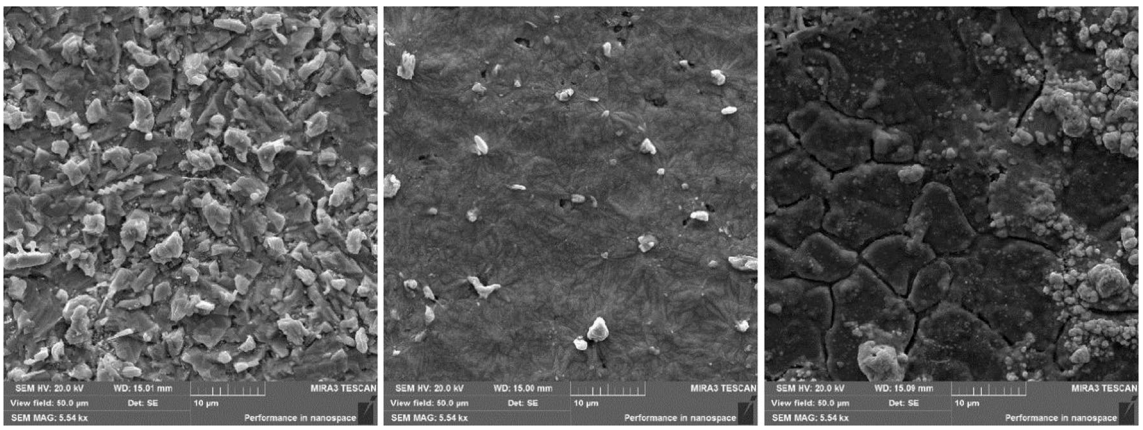

Fig. 10 SEM images of tin surface of the DC sample, (50 μm view field). Left panel – before argon plasma interaction, middle panel – majority of sample surface area after argon plasma interaction, right panel – minority of sample surface area close to the tin/steel boundary after argon plasma interaction (For plasma interactions the pressure is 1.5 Pa and Ar flow rate is180 sccm)

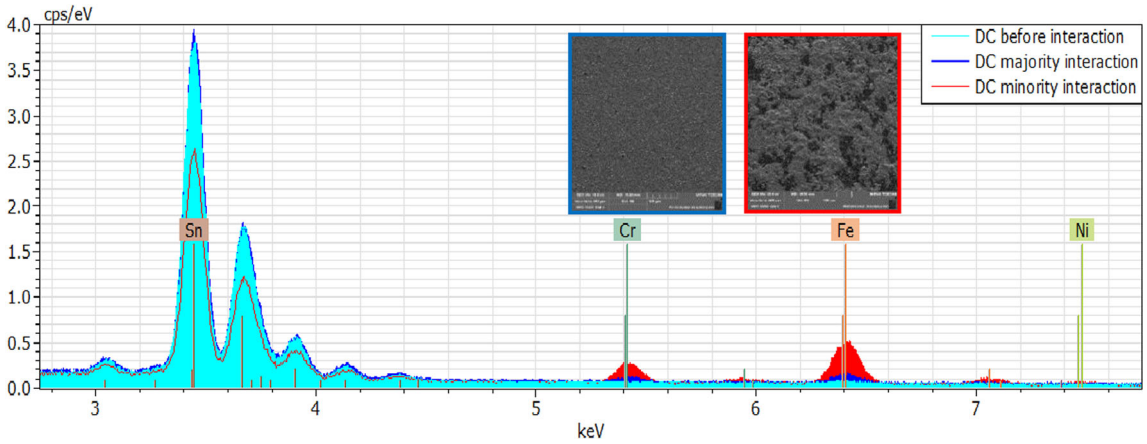

Fig. 11 Comparison of the EDS spectrum of the DC sample before and after 60 min plasma interaction. Insets, SEM images after plasma interaction, 500 μm view field. Left inset, majority sample area, right inset minority sample area (for explanation see text)

structure. Simultaneously, one observes also increase of intensity of Fe and Cr peaks, which are present in the stainless-steel substrate. In the minority of the sample surface area, we detect a promising change in EDS spectrum—the intensity of Sn peak is reduced by 33% is accompanied by a substantial increase in the intensities of peaks for substrate materials (Fe, Cr). We can argue that in this sample surface area the surface thickness has changed significantly. The measurement of film thickness post plasma exposure were approximately around 0.5 micron.

As for the sample prepared with hybrid HiPIMS the magnitude of the change after plasma interaction is more severe compared to the DC sample. In Fig. 12 we depict the SEM images of the hybrid HiPIMS sample in a manner like Fig. 10. Before interaction, left panel in Fig. 12, the tin film has very regular crystals, but due to the lower deposition rate of hybrid HiPIMS process the tin layer is not as thick as of DC sample which is around 1.5–2 micron. This can be observed on EDS spectrum of a hybrid HiPIMS sample before interaction in Fig. 13. We see that the intensities of Fe and Cr peaks are approximately of the same magnitude as in case of a DC sample after interaction. However, majority of the interacted sample surface, middle image in Fig. 12, has no bigger crystal, which were destroyed presumably due to high temperature. Consequently, appearance of the ripple effect is not as obvious as in DC sample. Nevertheless, the change in EDS spectrum after interaction is more significant than for DC sample. Tin peak is nearly half the intensity and intensities of Fe and Cr are almost factor three higher. This indicates that a comparatively large portion of tin film was removed from the surface.

The minority of surface after plasma interaction, right panel in Fig. 13, has a lot of similarities to minority of surface area after plasma interaction in DC sample. The main difference being that it is observed approximately in the middle of the sample surface, whereas for the DC sample this area was found close to the edges of tin surface.

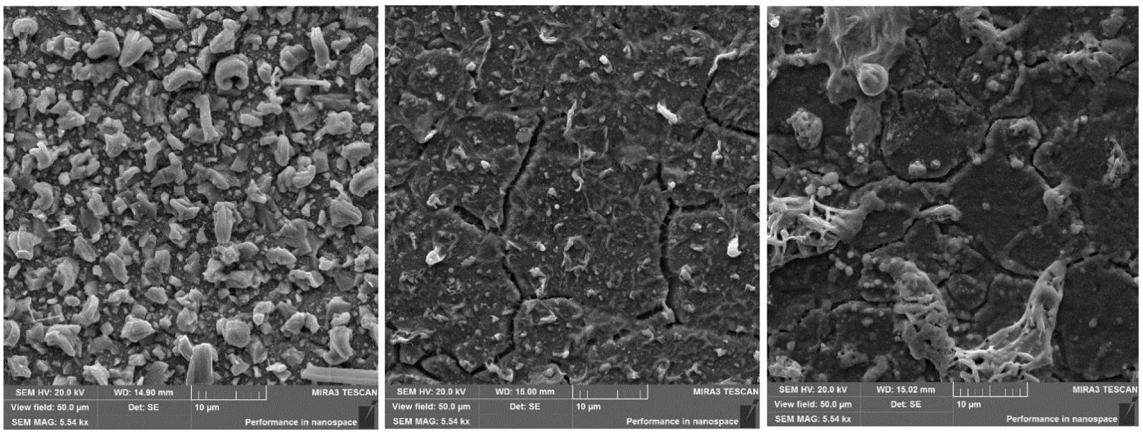

Fig. 12 SEM images of tin film surface of HiPIMS samples (50 μm view field) Left panel – before argon plasma interaction, middle panel – majority of sample surface area after argon plasma interaction, right panel – minority of sample surface area after argon plasma interaction (For plasma interactions the pressure is 1.5 Pa and Ar flow rate is180 sccm

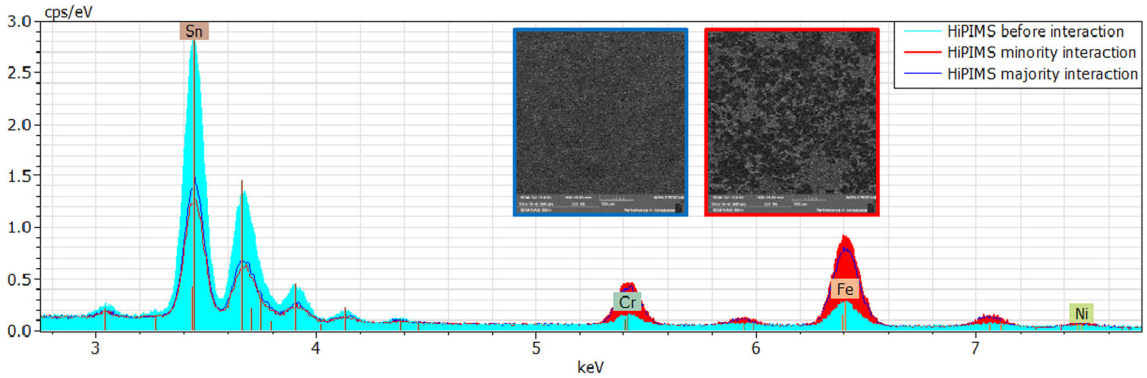

Fig. 13 Comparison of the EDS spectrum of the HiPIMS sample before and after 60 min plasma interaction. Insets, SEM images after plasma interaction, 500 μm view field. Left inset, majority sample area, right inset minority sample area (for explanation see text)

Nevertheless, this surface has areas where there is very small coating of tin and bigger melted tin island that are degraded due to ion interaction. Unfortunately, the difference of these two interactions is not that distinguishable on EDS spectrum of Fig. 13 because of the size of tested area, in which smaller regions with minority of surface after plasma interaction are separated by regions of majority of surface after plasma interaction.

This fact is best demonstrated in Fig. 14 with a bigger view field 1 mm. We see that areas of minority surface interactions are interlaced with island of majority surface.

Surface Morphological Study for Thin Tin Film Without Ion Bombardment

In this section we present results of substrate heating without plasma ion bombardment. We depict in Fig. 15 the SEM images of DC and HiPIMS samples after heating above melting point of tin at 242.5 °C for 30 min. We can clearly see the tin film on both samples.

The EDS spectrum in Fig. 16 compares the presence of tin in DC sample after plasma interaction and after just heating. We clearly see a lower amount of tin after plasma interaction compared to that after heating. Similar spectrum for the HiPIMS sample is shown in Fig. 17. This proves that in our case most of the tin removal has been achieved via ion bombardment.

Conclusion

One of the problems of the liquid metal tokamak divertor technology is the redeposition of the released metal on the tokamak vessel walls. We have demonstrated the successful removal of tin by low-pressure arc argon plasma in a hot cathode system. We believe that our system could be in principle used in tokamaks without a steady magnetic field. The Langmuir probe shows variations of the electron density and electron temperature with the distance from the chamber axis without and with substrate holder inside chamber. In case of absence of substrate holder, the electron density decreases with increasing distance from the chamber axis while electron temperature reaches a rather low value at the chamber axis, 0.93 eV, due to the proximity of the hot cathode. However, when substrate was inserted into the chamber rise of electron density is

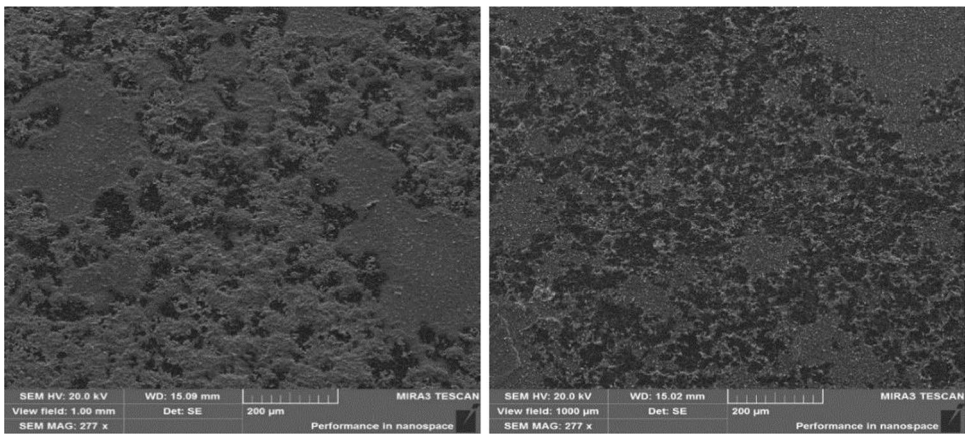

Fig. 14 SEM images for minority surface interaction of DC sample (left) and HiPIMS sample (right) after 60 min interaction with argon plasma, view field 1 mm. (for plasma interactions the pressure is 1.5 Pa and Ar flow rate is180 sccm)

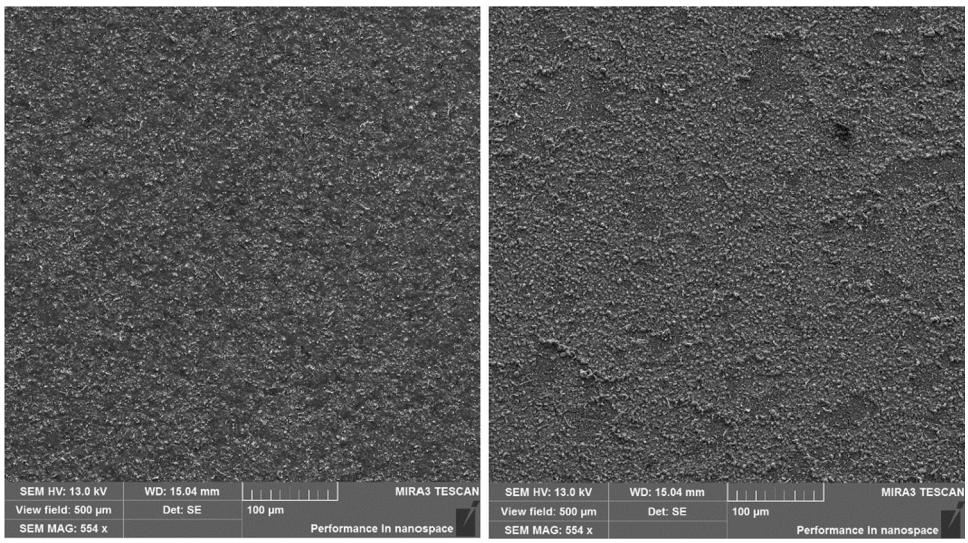

Fig. 15 SEM images of DC sample (left) and HiPIMS sample (right) heated above melting point of tin at 242 °C for 30 min

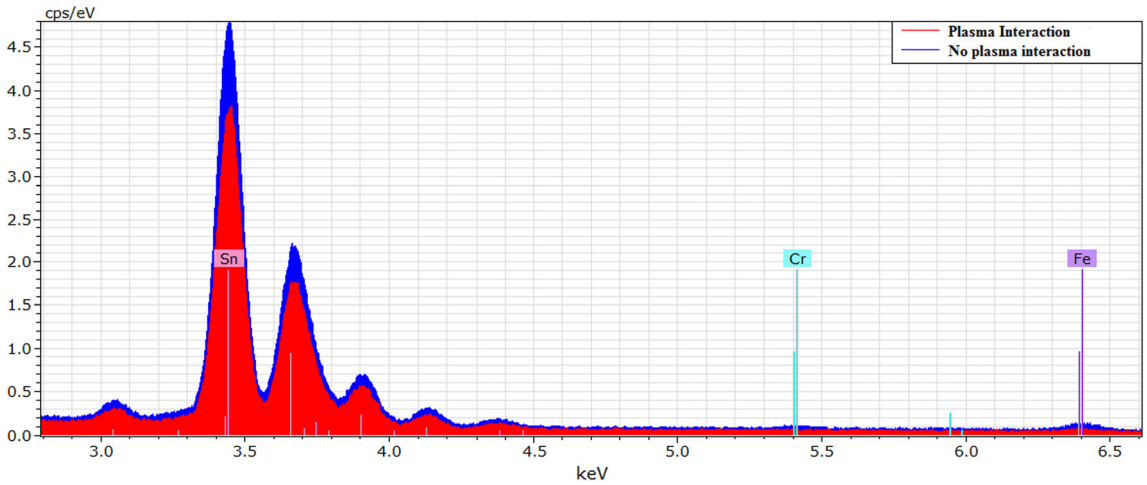

Fig. 16 EDS images DC sample heated for 242 °C above melting point of tin

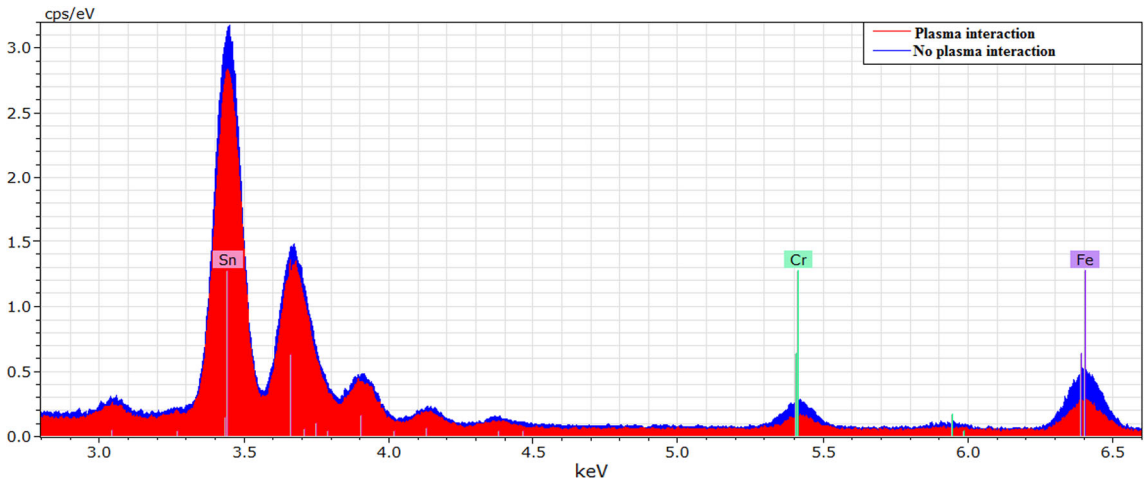

Fig. 17 EDS images HiPIMS sample heated for 242 °C above melting point of tin

accompanied by the decrease of electron temperature, which is almost constant with the distance from the axis. For morphological study of thin tin film SEM being deployed. The images clearly depict the removal of tin in case of both DC and hybrid HiPIMS prepared substrate. Due to the lower deposition rate of hybrid HiPIMS process the tin layer is not as thick as of DC sample which was clearly shown in EDS. Also, appearance of the ripple effect is not prominent in hybrid HiPIMS as in DC sample. The elemental composition proved presence of tin through EDS. In EDS the change in spectrum after interaction is more significant than for DC sample. Tin peak is nearly half the intensity and intensities of Fe and Cr are almost factor three higher. Thus, this study confirms comparatively large portion of tin film was removed from the surface.

The plasma diagnostic by optical emission spectroscopy shows presence of tin lines which are as follows: Sn I 365.5 nm, Sn I 380.1 nm, Sn I 452.5 nm, Sn II 805.5 nm, Sn I 811.4 nm. The most intensive Sn emission comes probably from a vapor cloud above the tin layer surface formed by evaporated, sputtered, and ionized tin atoms from the thin layer. We believe that this vapor cloud plays a key role in the high re-deposition rate.

The present study has shown that it is possible to remove a decent thickness of the tin layer using the ion bombardment from the low-temperature plasma. We are convinced that a continuation of present study can deepen the knowledge of plasma interaction with tin surface with prospective application in tokamaks without a steady magnetic field.

Acknowledgements This work was partial financial supported by Czech Science Foundation, Grant No. 24-10156S. The authors is grateful to RNDr. Adolf Kaňka Dr. for his informative discussion and useful recommendation in the field of optical emission spectroscopy.

Author contributions Conceptualization, [MT]; Methodology, [TH], [TM], [ZT], [MT]; Validation, [TH], [MT], [PK] and [MČ]; Investigation, [TH], [ZT], [TM], [MT] and [MČ]; Data curation, [TH], [TM], [ZT], [MT]; Writing—original draft preparation, [TH] , [MČ], [TM] and [MT]; Writing—review and editing, [TH] and [MT]; Supervision, [MT] and [MČ]; Project administration, [MT] and [ZH] All authors have read and agreed to the published version of the manuscript.

Data Availability The datasets are available from the corresponding author on a reasonable request.

Declarations

Conflict of interest The authors declare no conflict of interest.

References

1. K. Ioki, A. Cardella, I. Elio, Y. Gohar, T. Iizuka, G. Johnson, G. Kalinin, D. Lousteau, K. Mohri, R. Parker, R. Raffray, R. Santoro, K. Shimizu, N. Tachakawa, T. Takahashi, D. Williamson, E. Zolti, In Proceedings of 16th International Symposium on Fusion Engineering, vol. 1 (Champaign, 1995), p. 150
2. D.K. Yang, L.Y. Liao, Y.H. Li, G.Q. Zhong, X.J. Zhang, W. Zhang, B.L. Hao, L.Q. Hu, B.N. Wan, Z.M. Hu, Y.M. Zhang, G. Gorini, M. Nocente, M. Tardocchi, X.Q. Li, C.J. Xiao, T.S. Fan, Rev. Sci. Instrum. **93**, 113501 (2022)
3. N.A. Puntakov, A.A. Ayrapetov, L.B. Begrambekov, A.V. Grunin, S.S. Dovganyuk, A.S. Kaplevskiy, A.V. Tenishev, S.A. Grashin, I.I. Arkhipov, J. Phys. Conf. Ser. **1686**, 012014 (2020)
4. A.J.H. Donné, Philos. Trans. A Math. Phys. Eng. Sci. **377**, 20170432 (2019)
5. W. Biel, M. Ariola, I. Bolshakova, K.J. Brunner, M. Cecconello, I. Duran, Th. Franke, L. Giacomelli, L. Giannone, F. Janky, A. Krimmer, R. Luis, A. Malaquias, G. Marchiori, O. Marchuk, D. Mazon, A. Pironti, A. Quercia, N. Rispoli, S. El Shawish, M. Siccinio, A. Silva, C. Sozzi, G. Tartaglione, T. Todd, W. Treutterer, H. Zohm, Fusion Eng. Des. **179**, 113122 (2022)
6. P. Rindt, J. Mata González, P. Hoogerhuis, P. van den Bosch, M. van Maris, D. Terentyev, C. Yin, M. Wirtz, N.J. Lopes Cardozo, J.A.W. van Dommelen, T.W. Morgan, Using 3D-printed tungsten to optimize liquid metal divertor targets for flow and thermal stresses. Nucl. Fusion **59**(5), 054001 (2019). https://doi.org/10.1088/1741-4326/ab0a76
7. S. Roccella, G. Dose, R. de Luca, M. Iafrati, A. Mancini, G. Mazzitelli, J. Fusion Energ. **39**, 462 (2020)
8. F.L. Tabarés, E. Oyarzabal, A.B. Martin-Rojo, D. Tafalla, A. de Castro, A. Soleto, Nucl. Fusion **57**, 016029 (2017)
9. T.W. Morgan, P. Rindt, G.G. van Eden, V. Kvon, M.A. Jaworksi, N.J. Lopes Cardozo, Plasma Phys. Control Fusion **60**, 014025 (2018)
10. J. Horacek, S. Entler, P. Vondracek, J. Adamek, D. Sestak, M. Hron, R. Panek, R. Dejarnac, V. Weinzettl, K. Kovarik, G. Van Oost, Plasma Phys. Rep. **44**, 652 (2018)
11. V. Kvon, R. Al, K. Bystrov, F.J.J. Peeters, M.C.M. van de Sanden, T.W. Morgan, Nucl. Fusion **57**, 086040 (2017)
12. J.H. You, G. Mazzone, E. Visca, Ch. Bachmann, E. Autissier, T. Barrett, V. Cocilovo, F. Crescenzi, P.K. Domalapally, D. Dongiovanni, S. Entler, G. Federici, P. Frosi, M. Fursdon, H. Greuner, D. Hancock, D. Marzullo, S. McIntosh, A.V. Müller, M.T. Porfiri, G. Ramogida, J. Reiser, M. Richou, M. Rieth, A. Rydzy, R. Villari, V. Widak, Fusion Eng. Des. **109**, 1598 (2016)
13. V. Pericoli Ridolfini, P. Chmielewski, I. Ivanova-Stanik, M. Poradziński, R. Zagórski, R. Ambrosino, Phys. Plasmas **27**, 112506 (2020)
14. W. Ou, F. Brochard, T.W. Morgan, Nucl. Fusion **61**, 066030 (2021)
15. A. Manhard, T. Schwarz-Selinger, M. Balden, T. Dürbeck, H. Maier, R. Neu, Nucl. Fusion **60**, 106007 (2020)
16. A. Cremona, E. Vassallo, E. Alves, F. Causa, S. De Iuliis, R. Dondè, G. Giacomi, G. Gervasini, G. Granucci, M. Iafrati, G. Maddaluno, R. Mateus, D. Minelli, V. Mellera, A. Nardone, M. Pedroni, D. Ricci, V. Rigato, N. Rispoli, A. Uccello, Nucl. Mater. Energy **17**, 253 (2018)
17. T.W. Morgan, D.C.M. Van den Bekerom, G. De Temmerman, J. Nucl. Mater. **463**, 1256 (2015)
18. N. Matsunami, Y. Yamamura, Y. Itikawa, N. Itoh, Y. Kazumata, S. Miyagawa, Kenji Morita, R. Shimizu, H. Tawara, Energy dependence of the ion-induced sputtering yields of monatomic solids. Atom. Data Nucl. Data Tables **31**(1), 1–80 (1984). https://doi.org/10.1016/0092-640X(84)90016-0

19. P. Sigmund, Sputtering by ion bombardment theoretical concepts, in *Sputtering by Particle Bombardment I*. ed. by R. Behrisch (Springer Berlin Heidelberg, Berlin, Heidelberg, 1981), pp.9–71. https://doi.org/10.1007/3540105212_7
20. J. Roth, W. Moller, Nucl. Instrum. Methods Phys. Res. B 7–8 (1985)
21. R.P. Doerner, M.J. Baldwin, D.G. Whyte, S. Krasheninnikov, J. Nucl. Mater. **313**, 383 (2003)
22. R.W. Conn, R.P. Doerner, F.C. Sze, S. Luckhardt, A. Liebscher, R. Seraydarian, D.G. Whyte, Nucl. Fusion **42**, 1060 (2002)
23. J.P. Allain, M.D. Coventry, D.N. Ruzic, J. Nucl. Mater. **313**, 641 (2003)
24. M.D. Coventry, D.N. Ruzic, J. Nucl. Mater. **1015**, 337 (2004)
25. M. Zanáška, J. Adámek, M. Peterka, P. Kudrna, M. Tichý, Phys. Plasmas **22**, 033516 (2015)
26. D. Lundin, M. Čada, Z. Hubička, J. Vac. Sci. Technol. A **34**, 041305 (2016)
27. H. Mishra, M. Tichý, P. Kudrna, Vacuum **205**, 111413 (2022)
28. M. Tichy, M. Sicha, P. David, T. David, Contrib. Plasma Phys. **34**, 59 (1994)
29. J. Bohdansky, J. Roth, H.L. Bay, J. Appl. Phys. **51**, 2861 (1980)
30. P.J. Kelly, R.D. Arnell, Vacuum **56**, 159 (2000)
31. J.G.A. Bitter, A study of erosion phenomena part I. Wear **6**, 1 (1963)
32. Z. Ye, X. Ma, A. Wu, P. He, Z. Wang, Q. Yan, J. Wei, K. Zhang, F. Gou, J. Fusion Energ. **39**, 86 (2020)
33. A. Kramida, Yu Ralchenko, J. Reader, NIST ASD Team, In *NIST Atomic Spectra Database*. (2021) https://doi.org/10.18434/T4W30Fver.5.9
34. J.S. Colligon, Vacuum **24**, 373 (1974)